Rumpled surface structure and lattice dynamics of NiO(001)

Tetsuaki Okazawa, Yoshihiro Yagi, and Yoshiaki Kido*
Department of Physics, Ritsumeikan University, Kusatsu, Shiga-ken 525-8577, Japan
(Received 27 December 2002; published 7 May 2003)

Rumpled surface structure and root mean square (rms) thermal vibration amplitudes of NiO(001) were determined by high-resolution medium energy ion scattering. The clean 1×1 surface was prepared by cleavage in the air and annealing at 500 °C for 40 min in O_2 pressure of 1×10^{-4} Torr. The interlayer distance between the top and second layer is contracted by $1.44\pm0.07\%$ and the top-layer Ni plane is displaced by 0.10 ± 0.01 Å toward the vacuum side relative to the top-layer O plane. The present result is consistent with the recent *ab initio* calculation based on the density functional theory using the local spin density approximation. We also determined the rms thermal vibration amplitudes of Ni and O atoms in the bulk and in the top layer. The result obtained is compared with that calculated using the pair potential proposed by Lewis and Catlow.

DOI: 10.1103/PhysRevB.67.195406 PACS number(s): 68.35.Ja, 61.85.+p

Nickel monoxide is a typical $3d$ transition metal oxide (TMO) with an antiferromagnet and has recently attracted growing attention. The electronic structure of the surface and interface is fairly different from that of the bulk[1–3] and thus he thin films and heterostructures might give some novel and prominent property such as giant magnetoresistance and superconductivity. In addition, the surface with defects provides a variety of active sites for chemisorption.[4] So, it is expected to be applied, for example, to a hydrogen fuel cell.[5] In a fundamental aspect, the electronic structure of NiO is a charge-transfer type insulator with strongly correlated *d* electrons. Its band gap is 4.3 eV and the upper edge of the valence band is predominantly of *p* character.[6] The above electronic nature has been recently clarified by scanning tunneling microscope (STM)[7] and also by *ab initio* calculation based on the local spin-density approximation.[8]

The NiO crystal has a NaCl-type structure and its lattice constant at room temperature is 4.17 Å. Concerning the surface structure of NiO(001), Welton-Cook and Prutton[9] reported that the top layer is contracted toward the inside of the order of 2% of a layer spacing ($d=2.085$ Å) and not rumpled on a scale detectable low energy electron diffraction (LEED) analysis. Nakatsugawa and Iguchi[9] calculated the displacements of Ni and O atoms by the two-dimensional polarizable point–ion shell model and concluded that the interlayer distance between the top and second layer is contracted by 1–2.5% and the top-layer O atoms are displaced considerably toward the vacuum side relative to that of the top-layer Ni atoms. In contrast, recent classical molecular dynamics calculation using a rigid ion potential showed outwards expansion of Ni and inwards contraction of O atoms.[10] More recently, an *ab initio* calculation based on the density functional theory (DFT) using the local spin density approximation was performed and concluded a contraction of 1.3% and an inward displacement of O relative to Ni atoms in the top layer.[11]

In this study, we determine directly the surface relaxation and rumpling of NiO(001) by high-resolution medium energy ion scattering (MEIS). The displaced lattice positions of the top-layer O and Ni atoms scaled from the second-layer Ni are measured using the ion shadowing effect. The displaced lattice positions determined here are compared with the theoretical predictions.[9–11] We derive the dipole moments of the top-layer O and Ni atoms self-consistently assuming that O^{2-} and Ni^{2+} ions are located at the lattice sites and have polarizability of 2.61 and 0.05 $Å^3$, respectively. Then total potential energy is calculated for the top-layer atoms employing the pair potential proposed by Lewis and Catlow.[12] The applicability of the pair potential is judged from consistency or inconsistency between the observed lattice positions of the top-layer atoms and those minimizing the potential energy. The ion shadowing effect also allows us to extract the root mean square (rms) thermal vibration amplitudes (TVA's) of O and Ni atoms in the bulk and in the top layer. We calculate the bulk TVA's using the above pair potential and discuss the applicability of pair potentials to the NiO crystal.

The MEIS measurement was performed using a high-resolution toroidal electrostatic analyzer (ESA) under an ultrahigh vacuum (UHV) condition ($\leqslant2\times10^{-10}$ Torr). The clean NiO(001) surface was prepared by cleavage in the air and annealing at 500 °C in O_2 pressure of 1×10^{-4} Torr for 40 min. The latter annealing process is indispensable to eliminate the adsorbed carbon on the surface. The clean 1×1 surface was confirmed by reflection high energy electron diffraction (RHEED) and Auger electron spectroscopy. The sample was mounted on a six-axis goniometer and analyzed *in situ* by MEIS using well-collimated 120-keV He^+ beams. The backscattered He^+ ions were detected with the toroidal ESA mounted on a turntable, whose energy resolution ($\Delta E/E$) is 9×10^{-4}.

Figure 1 shows typical MEIS spectra observed for 120-keV He^+ ions incident along the [101] axis and also along the direction 1.5° off from the [101] axis and backscattered to 80° (random direction). We can clearly see the scattering components from three isotopes of ^{58}Ni, ^{60}Ni, and ^{62}Ni. The observed spectra are decomposed into three components from the top, second-, and third-layer Ni atoms, indicated by thin solid curves. For the off-axis incidence, the scattering component from the second layer is strongly increased due to a focusing effect. From these two spectra, the peak position and its energy spread are estimated accurately. We put two energy windows corresponding to the scattering components mainly from the second-layer Ni and from deeper layers Ni atoms. Then two angular scans were performed around the [111] axis in the (110) plane and around the [211] axis in the

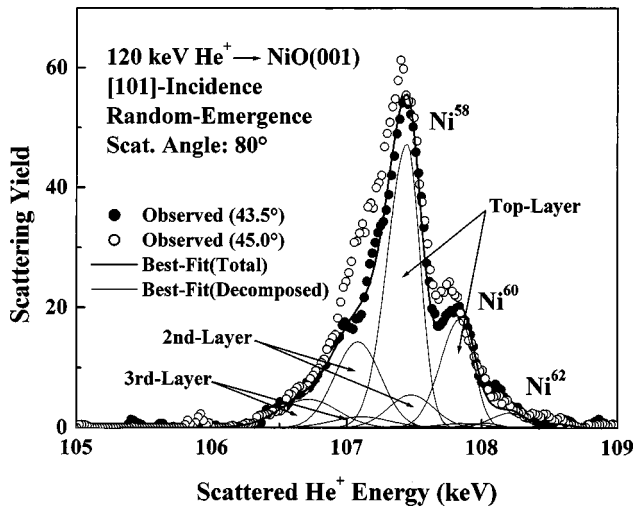

FIG. 1. MEIS spectra observed for 120-keV He^+ ions incident along the [101] axis (full circles) and along the direction 1.5° off from the [101] axis (open circles) and backscattered to 80° from Ni atoms of NiO(001). Thick and thin solid curves are best-fitted total and decomposed spectra from the top-, second-, and third-layer Ni atoms, respectively.

$(\bar{1}20)$ plane. The second-layer Ni atoms are shadowed by the top-layer O and Ni atoms, respectively, for the [111] and [211] incidence. Figure 2 shows the angular scan spectra around the [111] (upper) and [211] (lower) axis. The angles giving the scattering yield minima were determined by an appropriate polynomial fitting. The heights of the top-layer O and Ni atoms scaled from the second-layer Ni were derived from the angular shifts from the [111] and [211] axis using the simple triangulation method.[13] As the result, the top-layer O and Ni atoms are displaced by 0.08 ± 0.01 Å toward the inside and by 0.02 ± 0.01 Å toward the vacuum side, respectively. If we neglect the second-layer rumpling, the interlayer distance between the top and second layer is contracted by $1.44\pm0.7\%$ and the rumpling of the top layer is $-4.8\pm0.5\%$. The second-layer rumpling of 1% generates an error of 0.5% in the above relaxation value. The present result of the relaxation is quite consistent with the LEED analysis[9] and also with the shell model (1–2.5%)[10] and *ab initio* DFT (1.3%) calculations.[11] Concerning the rumpling of the top layer, our MEIS result clearly support the DFT prediction (-2.5%)[11] but it is in conflict with the shell model calculation.[10] The usual shell models have been successfully applied to alkali halide crystals but not to covalent crystals. It must be noted that NiO has both ionicity and covalency.[14,15]

Now, we check the applicability of pair potentials, which are frequently employed to reproduce the elastic quantities of ionic and metallic crystals. First, we derive the dipole moments of the top-layer O and Ni self-consistently assuming the displaced lattice positions determined by MEIS and the polarizability of O^{2-} $(2.61\times10^{-24}$ $cm^3)$ and Ni^{2+} $(0.05\times10^{-24}$ $cm^3)$.[15,16] The detail of this method is referred to the literature.[17] The dipole moments of the top-layer O^{2-} and Ni^{2+} were determined to be $+0.22$ and -0.065 in debye units $(10^{-18}$ esu cm), respectively. Lewis and Catlow proposed Born-Mayer-type potentials based on the shell model for metal oxides which reproduce the elastic constants and

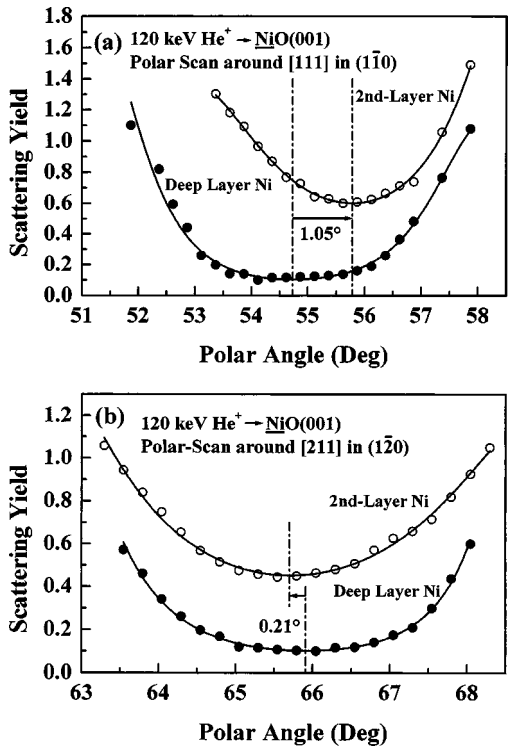

FIG. 2. (a) Polar scan spectra around the [111] axis in the $(\bar{1}10)$ plane for the scattering components from the second-layer (open circles) and from deep layers (full circles) Ni atoms. (b) Polar scan around the [211] axis in the (120) plane for the scattering components from the second-layer (open circles) and from the deep layers (full circles) Ni atoms.

diffusion activation energies for cation and anion.[12] We employed this pair potential for NiO and calculated total potential energies for the top-layer O and Ni independently as a function of the shift of the top O and Ni plane from the equilibrium lattice positions determined by MEIS (Fig. 3).

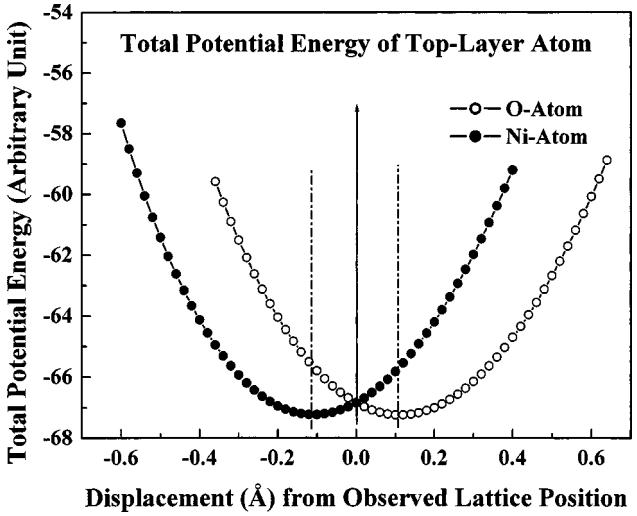

FIG. 3. Total potential energy for top-layer O (open circles) and Ni (full circles) as a function of displacement from the equilibrium lattice positions determined by MEIS. When the O plane (Ni plane) is shifted, the Ni plane (O plane) is fixed to the equilibrium position.

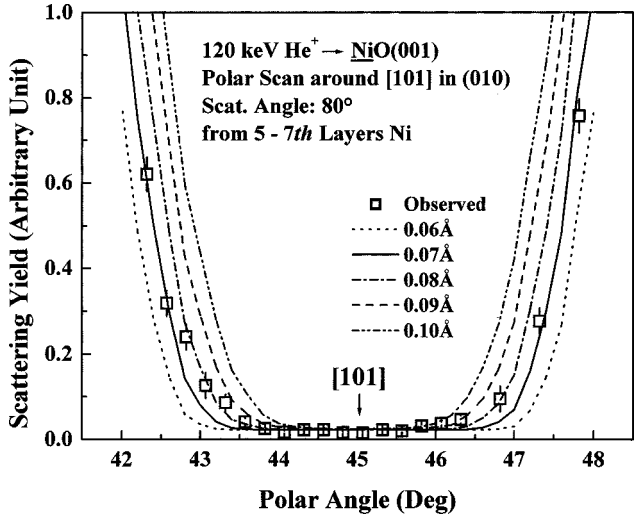

FIG. 4. Observed (squares) and simulated (curves) polar scan spectra around the [101] axis in the (010) plane for scattering components mainly from the fifth- to seventh-layer Ni atoms.

Here, the O^{2-} and Ni^{2+} states were assumed and the dipole moments derived previously were used. The displacements and the dipole moments of deeper layer atoms were neglected, because the deeper the lattice site position, the smaller the electric fields. The positions of the O and Ni planes minimizing the potential energy are largely deviated by more than 0.1 Å from the equilibrium positions. In the case of alkali halide crystals (KI and RbI), the deviations were found to be very small less than 0.04 Å. Such large deviations cannot be diminished by changing the polarizability and the ionic charge, because the primary contribution comes from the pair potential. To change the pair potential significantly leads to deviations of the calculated elastic constants and other lattice properties from the experimental values. The above discrepancy suggests a considerable contribution of covalency to the NiO crystal bonding.

We also determined the TVA's of the O and Ni atoms in the bulk and in the top layer by high-resolution MEIS. As reported previously,[17] the polar scan profile for the scattering components from deep layers atoms does not depend significantly on the correlations and enhancement of TVA's. Figure 4 shows the polar scan profile around the [101] axis in the (010) plane observed for the scattering components mainly from the fifth- to seventh-layer Ni atoms. The observed profile is compared with that calculated by Monte Carlo simulation of the ion trajectories assuming the rms TVA value of the bulk Ni atoms (0.06–0.10 Å: one-dimensional). Here, it must be noted that the [101] string consists of Ni or O atoms only. Apparently, the one-dimensional rms TVA of 0.075 $\pm$0.005 Å gives the best fit to the observed profile. It is difficult to perform a similar angular scan for the scattering components from deep layers O atoms, because the spectra from O atoms appear at a lower energy side and the scattering yields are very small compared with those for Ni atoms.

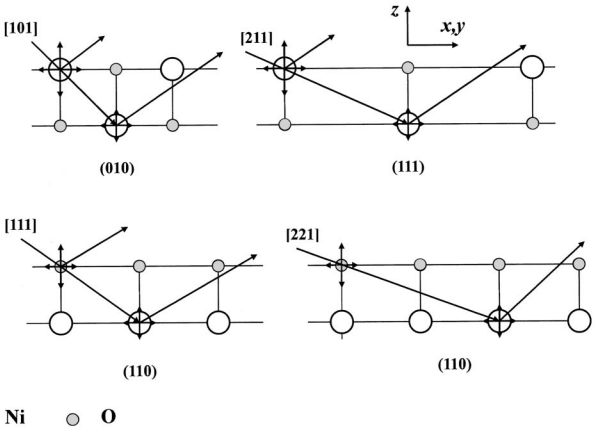

FIG. 5. Side view of various scattering geometries. Large open circles and small gray circles denote Ni and O atoms, respectively.

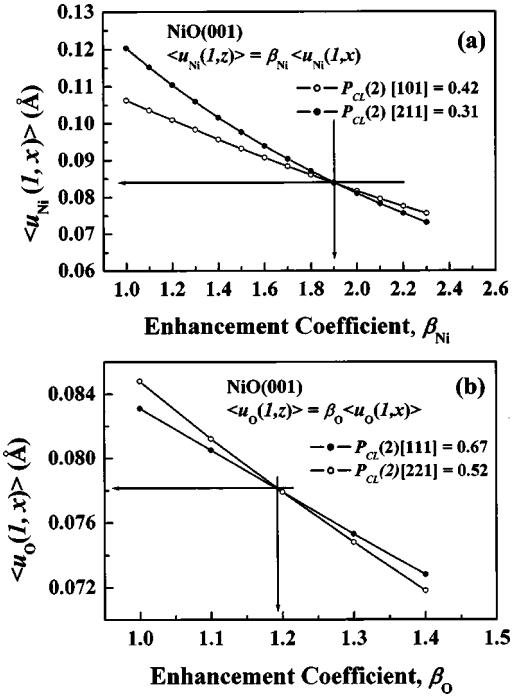

FIG. 6. (a) Points $(\langle u_{Ni}(1,x)\rangle, \beta_{Ni})$ satisfying the close encounter probabilities ($P_{CL}^{101}=0.42$, $P_{CL}^{211}=0.31$) for the second-layer Ni atoms for [101] and [211] incidence. The crossing point gives the $\langle u_{Ni}(l,x)\rangle$ and β_{Ni} values. (b) Points $(\langle u_O(1,x)\rangle, \beta_O)$ satisfying the close encounter probabilities ($P_{CL}^{111}=0.67$, $P_{CL}^{221}=0.51$) for the second-layer Ni atoms for [111] and [221] incidence. The crossing point gives the $\langle u_O(1,x)\rangle$ and β_O values.

Now we simplify the lattice motion and consider the enhanced TVA's of the top-layer atoms and correlations between the first nearest neighbors only. The TVA's of the deeper layer atoms are assumed to be the same as those of the bulk. We measured the MEIS spectra for [101], [211], [111], and [221] incidence and backscattering to random directions (see Fig. 5). The exact incident angles were chosen to minimize the scattering yield from the second-layer Ni atoms. Then the close encounter probabilities for the second-layer Ni were derived by decomposing the MEIS spectra. Here, the close encounter probability means the hitting probability normalized by that for the top-layer atoms which are not shadowed and thus it corresponds to the normalized scattering yield (the decomposed scattering yield from *n*th-layer atoms divided by that from the top-layer atoms). Under the

above scattering geometries, the close encounter probabilities for the second-layer Ni atoms were deduced to be 0.42, 0.31, 0.67, and 0.52 for [101], [211], [111], and [221] incidence, respectively. In the case of the [101] and [211] incidence, there are two fitting parameters, (i) TVA of the top-layer Ni atoms in the lateral plane $[\langle u_{\mathrm{Ni}}(1,x)\rangle]$ and (ii) that in the surface normal direction $[\langle u_{\mathrm{Ni}}(1,z)\rangle \equiv \beta_{\mathrm{Ni}}\langle u_{\mathrm{Ni}}(1,x)\rangle]$. The hitting probability for the second-layer Ni depends on the TVA's of the top-layer O and the second-layer Ni atoms. The latter is already known, because it is assumed to be equal to the TVA of the bulk. The combination $[\langle u_{\mathrm{Ni}}(1,x)\rangle, \beta_{\mathrm{Ni}}]$ satisfying the above close encounter probabilities are plotted in Fig. 6 (upper). The hitting probabilities (close encounter probabilities) were calculated by the Monte Carlo simulation of the ion trajectories considering the thermal vibrations of the lattice site ions. The crossing point gives just the real $\langle u_{\mathrm{Ni}}(1,x)\rangle$ and β_{Ni} values of 0.084 ± 0.003 Å and 1.90 ± 0.05, respectively. The lateral and vertical TVA's of the top-layer O atoms are also determined in a quite same manner. For the [111] and [221] incidence, the He^+ ions pass through in the vicinity of the top-layer O atoms and hit the second-layer Ni atoms with the above probabilities (see Fig. 5). So, the lateral $[\langle u_{\mathrm{O}}(1,x)\rangle]$ and vertical $[\langle u_{\mathrm{O}}(1,z)\rangle \equiv \beta_{\mathrm{O}}\langle u_{\mathrm{O}}(1,x)\rangle]$ TVA's of the top-layer O atoms are the fitting parameters. Figure 6 (lower) indicates the combination $(\langle u_{\mathrm{O}}(1,x)\rangle, \beta_{\mathrm{O}})$ satisfying each close encounter probability. The real $\langle u_{\mathrm{O}}(1,x)\rangle$ and β_{O} values are estimated to be 0.078 ± 0.002 Å and 1.20 ± 0.03, respectively. In contrast to the top-layer Ni atoms, the enhancement factor β_{O} is fairly small and close to unity. Therefore, the lateral TVA may be approximately equal to the TVA of the bulk O atoms. The present result shows almost the same TVA values of the bulk O and Ni and show pronounced enhancement of the TVA's of the top-layer Ni but not for the top-layer O atoms. It is intimately related to the fact that the top-layer Ni atoms are largely displaced toward the vacuum side relative to the top-layer O atoms.

We calculated the phonon dispersion relation and the density of states by solving the equation of motion for the bulk lattice site O and Ni atoms using the pair potential given by Lewis and Catlow.[12] Then the TVA's of the bulk O and Ni atoms were calculated to be 0.060 and 0.055 Å, respectively, considering the Planck distribution function. These calculated values are significantly smaller than the observed ones. In contrast, for alkali halide crystals (KI and RbI), the bulk TVA's calculated in a quite same manner using the pair potential proposed by Catlow, Diller, and Norgett[18] are in good agreement with the experimental ones determined by MEIS.[17] The present result suggests that usual shell model calculation is not adequate for NiO crystal which has significant covalency.

In summary, we determined the rumpled surface structure of NiO(001) by high-resolution MEIS. As the result, the interlayer distance between the top and second layer is contracted by $1.44\pm0.7\%$ and the top-layer Ni is displaced toward the vacuum side by 0.10 ± 0.01 Å relative to the top-layer O atoms. The former relaxation value is consistent with the LEED analysis and the shell model and *ab initio* calculations. Concerning the rumpling, the present MEIS result is consistent with the *ab initio* DFT prediction but in conflict with the shell model calculation. We checked the applicability of the pair potential deduced based on the shell model which reproduces the experimental elastic constants of NiO. The pair potential proposed by Lewis and Catlow did not reproduce the displaced surface structure determined by MEIS. We also determined the TVA's of the bulk and the top-layer O and Ni atoms using the ion shadowing effect. The TVA's of the bulk O and Ni are almost the same value around 0.080 Å. However, the TVA of the top-layer Ni is strongly enhanced and in contrast that of the top-layer O is slightly increased. It is probably due to the largely displaced top-layer Ni toward the vacuum side relative to the top-layer O atoms. The bulk TVA's of Ni and O calculated using the Lewis-Catlow pair potential are about 20% smaller than those determined by MEIS. The present result and discussion suggest that the usual shell model and pair potentials are not simply applicable to the NiO crystal with significant covalency.

The authors would like to thank Y. Hoshino for supporting the sample preparation and the MEIS experiment.

*Corresponding author. Email address: ykido@se.ritsumei.ac.jp

[1] M. A. van Veenendaal and G. A. Sawatzky, Phys. Rev. Lett. **70**, 2459 (1993).
[2] D. Alders, F. C. Voogt, T. Hibma, and G. A. Sawatzky, Phys. Rev. B **54**, 7716 (1996).
[3] D. Alders, L. H. Tjeng, F. C. Voogt, T. Hibma, G. A. Sawatzky, C. T. Chen, H. Vogel, M. Sacchi, and S. Iacobucci, Phys. Rev. B **57**, 11 623 (1998).
[4] J. M. Blaisdell and A. B. Kunz, Phys. Rev. B **29**, 988 (1984).
[5] Z. Zou, J. Ye, K. Sayama, and H. Arakawa, Nature (London) **414**, 625 (2001).
[6] G. A. Sawatzky and J. W. Allen, Phys. Rev. Lett. **53**, 2339 (1984).
[7] M. R. Castell, P. L. Wincott, N. G. Condon, C. Muggelberg, G. Thornton, S. L. Dudarev, A. P. Sutton, and G. A. D. Briggs, Phys. Rev. B **55**, 7859 (1997).
[8] S. L. Dudarev, A. I. Liechtenstein, M. R. Castell, G. A. D. Briggs, and A. P. Sutton, Phys. Rev. B **56**, 4900 (1997).
[9] H. Nakatsugawa and E. Iguchi, Surf. Sci. **357-358**, 96 (1996).
[10] T. E. Karakasidis, D. G. Papageorgius, and G. A. Evangelakis, Appl. Surf. Sci. **162-163**, 223 (2000).
[11] H. Momida and T. Oguchi, J. Phys. Soc. Jpn. **72**, 588 (2003).
[12] G. V. Lewis and C. R. A. Catlow, J. Phys. C **18**, 1149 (1985).
[13] T. Nishimura, A. Ikeda, H. Namba, and Y. Kido, Surf. Sci. **411**, L834 (1998).
[14] L. M. Peng, S. L. Dudarev, and M. J. Whelan, Phys. Rev. B **56**, 15 314 (1997).
[15] R. R. Reddy, Y. N. Ahammed, P. A. Azeem, and K. R. Gopal, J. Non-Cryst. Solids **286**, 169 (2001).
[16] K. S. Upadhyaya, G. K. Upadhyaya, and A. N. Pandey, J. Phys. Chem. Solids **63**, 127 (2002).
[17] T. Okazawa, T. Nishimura, and Y. Kido, Phys. Rev. B **66**, 125402 (2002).
[18] C. R. A. Catlow, K. M. Diller, and M. J. Norgett, J. Phys. C **10**, 1395 (1977).